2019 International Conference on Robotics and Automation (ICRA)
Palais des congres de Montreal, Montreal, Canada, May 20-24, 2019

Steering Co-centered and Co-directional Optical and Acoustic Beams with a Water-immersible MEMS Scanning Mirror for Underwater Ranging and Communication

Xiaoyu Duan, Dezhen Song, and Jun Zou

Abstract— **This paper reports the development of a compact optical-acoustic frontend module for underwater communication and ranging. The module is enabled by a new water-immersible MEMS scanning mirror (WIMSM). It is capable of transmitting, receiving and steering co-centered and co-directional laser and ultrasound beams under water. To monitor its rotating angle in real time, scan position sensors based on Hall effect have been integrated into the WIMSM. The angular alignment of the laser and ultrasound beams in both transmission and reception modes has been examined. The experimental results show that the laser and ultrasound beams can remain aligned with less than 2.1 degrees under envelope of pan and tilt rotations. This capability is critical for the continuing development of the new bi-modal communication and ranging underwater Vehicles (AUVs).**

I. Introduction

Today Autonomous Underwater Vehicles (AUVs) are very important tool for many applications including infrastructure inspection and maintenance[1], search and rescue[2], environmental monitoring[3], maritime archaeology[4], oil drilling and pipeline inspection, and defense, etc. However, a significant and fundamental challenge that AUVs have to face is communication and perception in the underwater environment. No effective cordless high-speed underwater communication exists. Untethered miniature AUVs exist [3][5] but they are very limited in capability also due to the communication and perception issues [6][7][8]. Most of them can only communicate with the base station via satellite links by surfacing periodically. There is almost no coordinated AUV team due to lack of inter-vehicle communication capabilities. Even if some AUVs may be able to talk to each other via acoustic channels, its low bandwidth significantly limits their application potential [9][10][11]. To address this issue, we propose a novel dual-modal oPtical and Acoustic communication and Ranging (PAIR) device to simultaneously transceive co-centered and co-directional laser and ultrasound beams driven by a single scanner.

We report the development of the frontend module of this PAIR device, a compact optical-acoustic bi-modal transceiver that generates/receives co-centered and co-directional laser and ultrasound signal beams (See). To ensuring co-centered and co-directional signal alignment is critical because it eliminates challenges in sensor fusion caused by perspective difference and different transmission paths in communication and ranging. The resulting bi-modal sensor can fully utilize the commentary nature of two signal modalities: an ultrasound beam has wide signal dispersion pattern (easy to acquire handshake), is short-sighted, and is slow in communication speed [12][13][14], while a laser beam has narrow signal dispersion pattern (difficult to acquire handshake), is far-sighted (i.e. cannot measure short distance), and is very fast in communication speed [15][16].

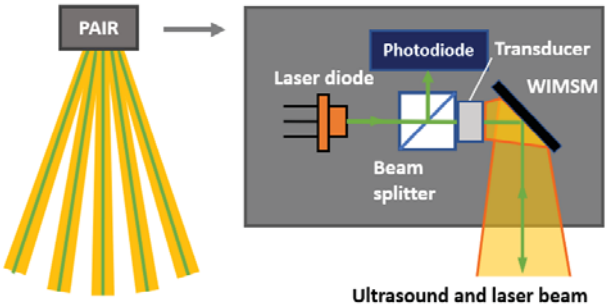

Fig. 1. Schematic design of the optical-acoustic frontend module for the PAIR device.

The main innovation of the frontend module is the seamless integration of these two signal modalities into a compact package with co-centered and co-directional steering. In current LiDAR systems, mechanical-scanning LiDAR requires accurate moving parts or extra scanner to increase sensor coverage [17], inevitably leading to bulky size and expensive cost. While chip-based solid-state LiDAR 'steers' the radio with photonic phased array [18][19], it cannot co-steer ultrasound beam. In comparison, MEMS-based LiDAR uses micro-mirrors to directionally control orientation of laser tranception. However, conventional MEMS scanning mirror are designed to operate in air and cannot be used to steer ultrasound beam underwater [20][21]. In recent years, we have developed novel water-immersible MEMS scanning mirrors (WIMSMs) [22][23][24]. In contrast to conventional MEMS scanning mirrors that, the WIMSMs are capable of fast steering both laser and ultrasound beams in water. This unique capability provides an ideal solution for the development of the optical-acoustic frontend module of the PAIR device. In this paper, we report the design, fabrication and testing of the

*The research is supported in part by National Science Foundation under NRI-1748161 and NRI-1526200.

X.Duan and J. Zou are with the Electrical and Computer Engineering Department, Texas A&M University, College Station, TX 77843, USA (e-mails: {duanxiaoyu, junzou}@tamu.edu).

D. Song is with the Computer Science and Engineering Department, Texas A&M University, College Station, TX 77843, USA (e-mails: dzsong@cs.tamu.edu).

optical-acoustic frontend module for the PAIR device. Especially, the transmission, reception, and steering of co-centered and co-directional laser and ultrasound beams have been experimental verified. The results show that the laser and ultrasound beams can remain aligned with less than 2.1 degrees under the operation envelope of pan and tilt rotations.

II. Design

The optical-acoustic frontend module for the PAIR device performs three main functions: optical transception, ultrasound transception, and co-centered and co-directional beam steering. These three functions can be configured into different operation modes, such as transmission, reception and pulse echo. The transmission and reception modes allow searching, aiming and communication between two PAIR devices, while the pulse-echo mode is useful for ranging.

illustrates the proposed system architecture for the optical-acoustic frontend module. The optical transceiver consists of a laser diode as light source, a photodetector and an optical beam splitter (OBS) to separate the transmitted and received laser signals. The ultrasound transceiver consists of a ring-like piezo transducer for both transmission and reception while allowing the laser to pass through. The relative position of the optical and ultrasound transceiver can be fine adjusted to achieve co-centered and co-directional laser and ultrasound beams. A WIMSM is used to provide beam steering around two orthogonal axes. For feedback control, the rotating angle of the reflecting mirror plate is monitored by an integrated scan position sensor.

III. Fabrication and Assembly

A. *Water-immersible MEMS scanning mirror*

As one of the key components in the optical-acoustic frontend module, the water-immersible MEMS scanning mirror steers the co-centered laser and ultrasound beams. (a) and (b) show the schematic design and a picture of a fabricated scanning mirror with an overall size of 40 mm × 40 mm × 20 mm. It consists of a reflective mirror plate, which is connected to an inner frame with a pair of flexible polymeric hinges. The inner frame is supported on an outer frame by a second pair of flexible polymeric hinges. This configuration provides the mirror plate with two rotational degrees of freedom around two orthogonal scanning axes. The mirror plate (20 mm × 20 mm) is diced from a silicon wafer and coated with a layer of aluminum to provide high reflectivity for both laser and ultrasound beams. Four electromagnetic actuators (each consisting of a permanent magnet and an inductor coil) are used to drive the scanning mirror. When a current is applying onto the coils, the generated magnetic field creates a force on the magnets to rotate the mirror plate around Y axis ("tilt") and the inner frame (together with the mirror plate) around X axis ("pan"). Driven by a 250-mA DC current, the scanning mirror can reach a rotating angle of $\pm$ 6.5° around X axis and $\pm$8.5° around Y axis, respectively. When driven at its resonance frequency (20 Hz for X axis and 12Hz for Y axis), similar titling angles can be reached with 176-mA AC driving current.

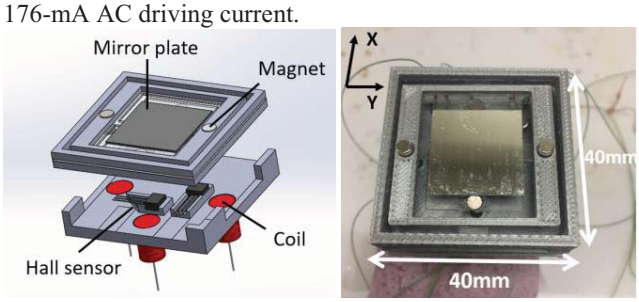

(a) (b)

Fig. 2. (a) Schematic design of WIMSM. (b) A photo of the fabricated device.

B. *Scan position sensor*

To monitor the rotating angle of the mirror plate, an integrated scan position sensor has been developed (). It consists of a small sensing magnet attached onto the mirror plate and a Hall sensor fixed underneath. When the mirror plate is tilted, the sensing magnet moves either closer or farther away from the Hall sensor, causing the magnetic field reaching the Hall sensor to increase or decrease. The relative rotating angle of the mirror plate can be determined by the variation of the voltage output of the Hall sensor. The relationship between the Hall sensor output and the distance between the Hall sensor and the sensing magnet has been characterized (Fig. 5 (a)). The Hall sensor output is saturated from 0 to 1.7 mm and then drops gradually at larger distance. Between 1.7 mm to 2.5 mm, the Hall sensor has the best sensitivity and also good linearity. As a result, the initial distance between the Hall sensor and the sensing magnet is set to 2.1 mm. Under this condition, the relationship between the Hall sensor output voltage and the rotating angle of the mirror plate has been characterized (Fig. 5(b)). The Hall sensor output voltage changes almost linearly with the rotating angle with an overall resolution of 60 mV/degree, which is adequate for both monitoring and feedback control of the rotating angle of the mirror plate.

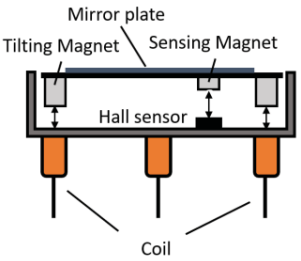

Fig. 3. Schematic cross-section of WIMSM showing the scan position sensor design.

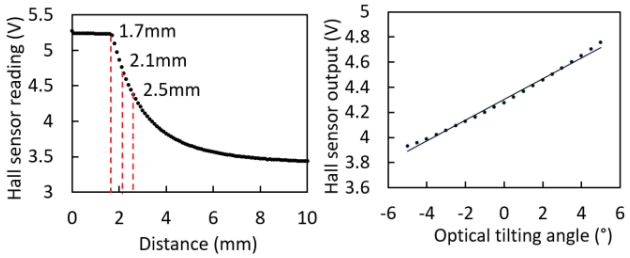

(a) (b)

Fig. 4. (a) Calibration curve of the Hall sensor. (b) The Hall sensor output voltage vs. the optical rotating angle of the mirror plate.

C. Ultrasound transducer

A custom-made ultrasound transducer is used to send and receive the ultrasound beam. It is made of a piezo ring with an outer diameter of 10 mm and an inner diameter of 6 mm. A polished acrylic quarter-wavelength matching layer with a thickness of 19 mm is bonded onto the piezo ring to improve its acoustic coupling with water.

For underwater ultrasound transception, the detection range depends on both attenuation and divergence of the ultrasound beam. The acoustic attenuation in water is related to the ultrasound frequency [25]. In general, higher frequency ultrasound has more attenuation. However, decreasing the frequency results in a larger diverging angle, which leads to a drop of receiving signal far from the transmitter. In this work, the resonance frequency of the piezo ring is chosen to be 330 kHz as a compromise between signal attenuation and divergence.

In order to determine its divergence, the radiation pattern of the ultrasound transducer in water has been characterized. As shown in Fig. 5(a), two identical transducers are used as the transmitter and receiver, respectively. They are placed face-to-face at a distance of 90 cm. The receiver is moved horizontally or vertically relative to the transmitter. At each scan point, the peak amplitude of the received ultrasound signal is recorded. (b) shows the normalize ultrasound intensity distribution in the horizontal (pan) direction, which indicates that the (half) -6 dB diverging angle is around 10° where amplitude drops to half of the peak value. The ultrasound attenuation is also tested by placing the receiving transducer at different distances from the transmitting transducer. The overall ultrasound attenuation is found to be ~2.2 dB/m.

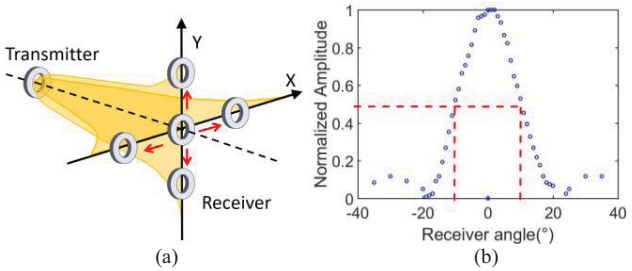

(a) (b)

Fig. 6. (a) Schematic of ultrasound beam mapping. (b) Measured ultrasound amplitude distribution in the horizontal (pan) direction.

D. Optical components

The optical components consist of a laser diode as transmitter, a photodiode as receiver, and an optical beam splitter (OBS), which are all commercially available. The sending and receiving beams are both divided by the OBS and only the latter is directed onto the photodiode. For underwater communication and ranging, a blue-green light is desirable because of lower attenuation in sea water. Here, the transmitter is a 5-mW 532-nm green laser diode. The photodiode has a detection area of 3.6 × 3.6 mm^2, an operation wavelength range of 350-1100 nm, and a responsivity of 0.65 A/W.

E. Assembly and adjustment

After their fabrication and testing, the WIMSM and ultrasound transducer are assembled into a 3D-printed frame with the optical components (). The overall size of the assembled module is 8 cm × 5.5 cm × 5 cm. To obtain the co-centered and co-directional laser and ultrasound beams, accurate alignment of the ultrasound transducer, laser diode and photodiode is required. To adjust the alignment of the ultrasound and laser beams, a reflecting mirror has been placed in front of the assembled module. A small pinhole is place at the center of the photodiode. The ultrasound transducer operates in the pulse-echo mode, while the laser diode is driven in the CW mode. The angular position of the reflecting mirror is carefully adjusted, such that the amplitude of the received ultrasound echo signal reaches its maximum. The orientation of the laser diode is fine-tuned by adjusting the four holding screws until the reflected laser signal received by the photodiode also reaches its maximum.

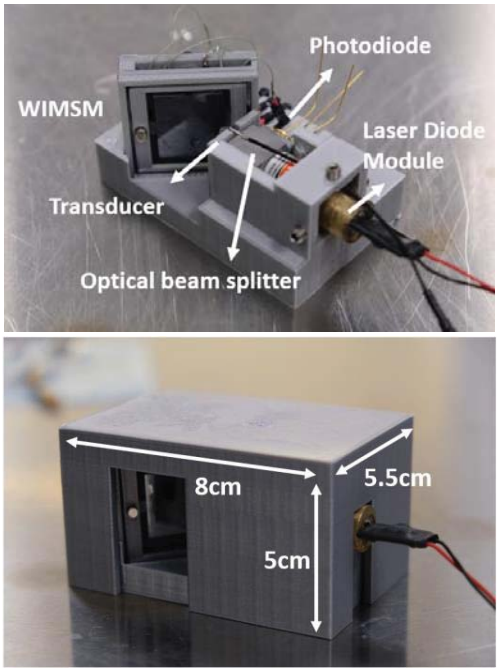

(a)

(b)

Fig. 7. An assembled optical-acoustic frontend module: (a) without cover and (b) with cover.

IV. Testing

The main goal of the testing is to characterize and verify the co-centered and co-directional alignment of the laser and ultrasound beams during transmission and reception. shows the test setup. Two frontend modules (one simplified and one complete) are placed inside a one-meter-long water tank. The complete module is fully equipped with all the components, while the simplified module has all optical and acoustic components except the WIMSM. A two-channel function generator is used to drive the WIMSM. The rotating angle of the mirror plate is monitored by the Hall scan position sensor. An ultrasound pulser/receiver is configured into the pulse-echo mode. It sends a driving voltage to the sending transducer (in the transmitting module) and amplifies the received ultrasound signal from the receiving transducer (in

the receiving module). A DC power supply is used to drive the laser diode (in the transmitting module) for sending a CW laser beam. The received laser and ultrasound signals from the receiving module are displayed on an oscilloscope.

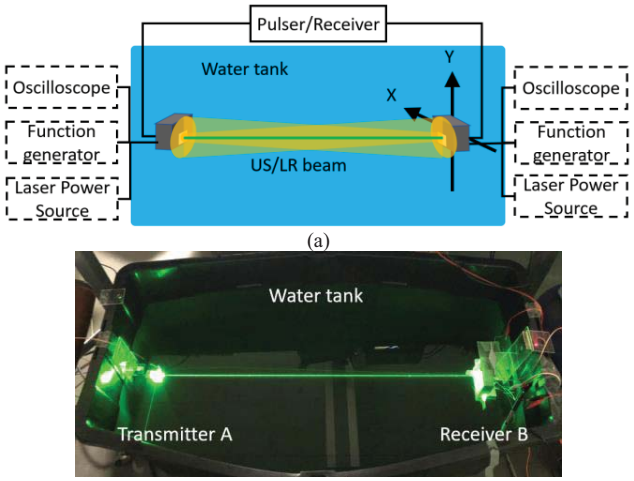

Fig. 8. (a) Schematic diagram of the testing setup for the optical-acoustic frontend module. (b) Actual view of the testing setup.

A. *Transmission Test*

In transmission test, the complete and simplified modules are configured as the transmitter and receiver, respectively. The transmitter sends a laser and ultrasound beam, which is co-steered by the built-in WIMSM in different directions. For each sending direction, the position of the receiver is adjusted to identify the two locations where the amplitude of the received laser and ultrasound signals reach their maximum, respectively (Fig. 8). Because the diameter of laser beam is much smaller than the detection area of the photodiode, a small pinhole is place at the center of the photodiode in the receiver to improve the locating accuracy of the laser beam. The shift of these two maximal amplitude locations is used to calculate the angular misalignment of the transmitted laser and ultrasound beam in one direction.

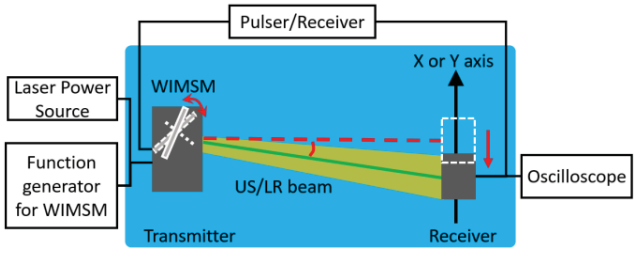

Fig. 9. Schematic diagram of the transmission test.

(a) shows the angular misalignment of the transmitted laser and ultrasound beams at different rotating angles of the mirror plate for pan rotations (around X axis). The minimal misalignment of 0.4° occurs at 0° rotating angle and slightly increases to 1.2~1.4° when the rotating angle reaches ±8.5°. (b) shows the angular misalignment of the transmitted laser and ultrasound beams for tilt rotations (around Y axis). The minimal misalignment of 0.35° occurs at 0° rotating angle and fluctuates between 0.4° and 0.65° when the rotating angle increases to ±6.5°. The slight increase in the misalignment at larger rotating angles for pan rotations can be explained by the fact that the mirror plate is placed at 45° across the laser and ultrasound beams. Both the laser and ultrasound beams undergo a 90° rotation when they are reflected by the mirror plate (See and). While the highly-collimated laser beam profile is largely not affected by the reflection, the center of the diverging ultrasound beam profile could be slightly shifted after the reflection. Furthermore, both pan and tilt rotations were applied to WIMSM to understand the mismatch on the detection plane. shows the error angle at each spot of 2-axis mirror rotation. The amount of shift and the resulting misalignment increases with the rotating angle of the mirror plate. The error reaches maximum of 2.1°, when pan and tilt rotations are 8° and 6° respectively. However, the overall misalignment still remains small over the entire scanning range of the WIMSIM.

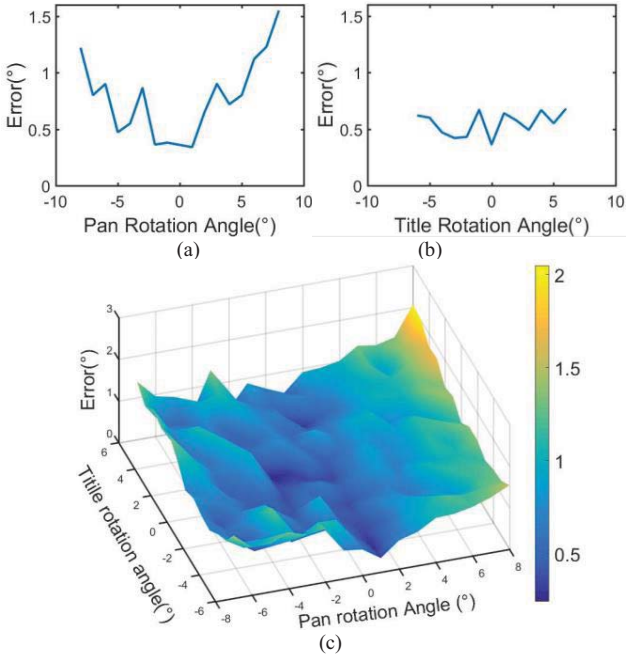

Fig. 10. Angular misalignment of the laser and ultrasound beams: (a) for pan rotation, (b) for tilt rotation, and (c) in the XY plane.

B. *Reception Test*

In reception test, the simplified and complete modules are configured as the transmitter and receiver, respectively (). The transmitter sends a laser and an ultrasound beam toward the receiver at a fixed direction. The WIMSM in the receiver is scanned at different angles around both X and Y axes. At each scan point, the amplitude of the received laser and ultrasound signals is recorded. First, the transmitter and receiver are aligned face to face (i.e., no angular offset) and the test is conducted three times to verify the repeatability of the reception of the laser and ultrasound signals. Next, the receiver is oriented at a set of offset angles (-6°, -1.5°, 1° and 4°) and the test is repeated.

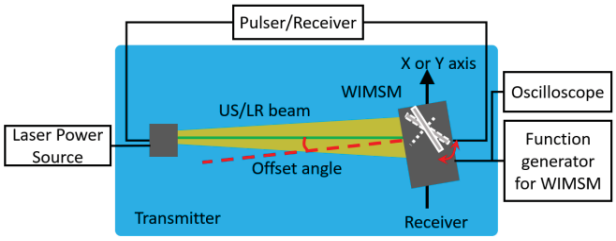

Fig. 11. Schematic diagram of the reception test.

(a) and (b) show the normalized amplitude of the received ultrasound signals as functions of the rotating angle of the mirror plate for pan and tilt rotations, respectively. For the ultrasound signal, its beam profile is similar to the characterized profile of the bare ultrasound transducer (see b), except some distortion or blockage caused by the reflection or scattering on the mirror frame at larger rotating and offset angles. The small deviation in ultrasound amplitude data obtained from the repeated tests at 0° offset indicates good repeatability of signal reception. The peak amplitude of the received ultrasound signals always occurs at the rotating angle that is equal to the offset angle of the receiver. This is because the rotating angle of the mirror plate has to compensate the offset angle for aiming the receiver to the incoming ultrasound beams for the best reception.

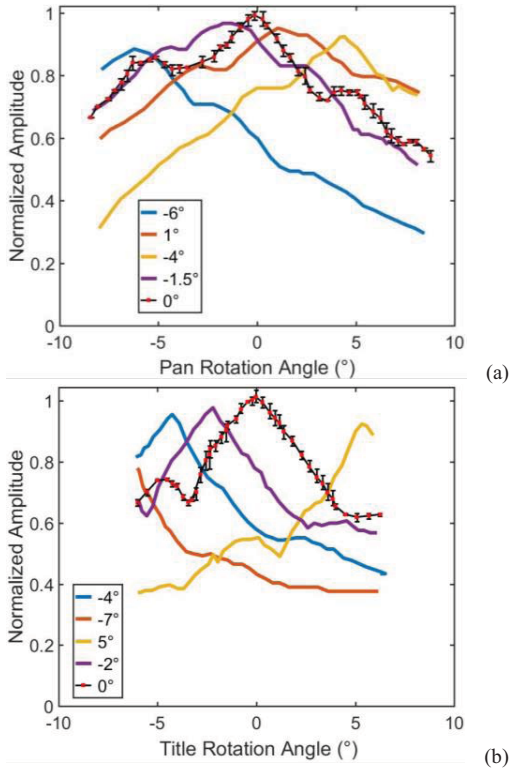

Fig. 12. Normalized amplitude of received ultrasound signals vs. mirror rotating angle at different offset angles: (a) for pan rotation and (b) for tilt rotation.

(a) and (b) show the normalized amplitude of the received laser signals as functions of the rotating angle of the mirror plate for pan and tilt rotations, respectively. For the laser signal, abrupt rise and fall occur when the mirror plate rotating angle is around -2.5° and 2.5°. Blockage of the laser signal by the mirror frame occurs at larger rotating and offset angles. From -2.5° to 2.5°, the amplitude of the laser signal remains almost constant. This indicates that the laser beam can be well received within ±2.5°, which is due to the much larger diameter of the photodiode active area than that of the cross-section of the laser beam (). As the receiver, the optical-acoustic frontend module can have a tolerance ±2.5° for the misalignment of the laser and ultrasound beams. This feature is especially beneficial for using the ultrasound beam to search and aim the laser beam to pair laser transceivers for high speed communication.

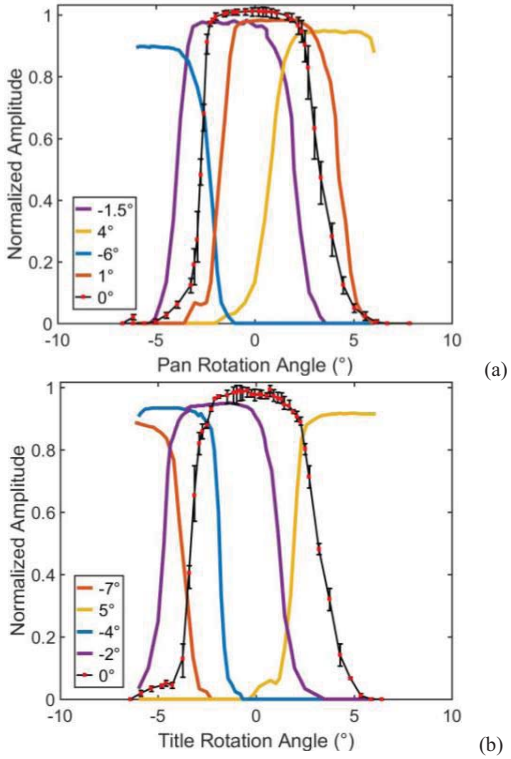

Fig. 13. Normalized amplitude of received laser signals vs. mirror rotating angle at different offset angles: (a) for pan rotation and (b) for tilt rotation.

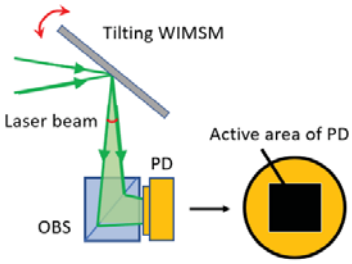

Fig. 14. Illustration of the effective laser transception area based on the photodiode active area.

V. Conclusion

In conclusion, we have successfully designed and tested a new and compact optical-acoustic frontend module, which is capable of transmitting, receiving and steering co-centered and co-directional laser and ultrasound beams under water. Ensuring the precise signal alignment was critical in enabling bi-modal communication and ranging. We have reported

design details which include a two signal tranception channels and WIMSM-based biomodal scanning. Our test results show that we have achieved satisfying signal alignment of less than 2.1 degrees in the pan and tilt operation range.

This work is expected to build a technical foundation and form the first step for the development of the proposed PAIR device. In the future, the scanning range of the WIMSM will be improved to enhance the searching and aiming capability. An integrated hardware and software interface will be developed for control and data acquisition. A Medium Access Control (MAC) layer will be developed. The system's dynamic performance under real working conditions will be tested. In addition, new pulsed light and ultrasound sources will be investigated to enable the ranging functions as well.

ACKNOWLEDGMENT

The authors thank D. Wang and C. Fang for their inputs and help in experiments.

REFERENCES

[1] F. S. Hover et al., "Advanced perception, navigation and planning for autonomous in-water ship hull inspection," Int. J. Rob. Res., vol. 31, no. 12, pp. 1445–1464, 2012.

[2] H. Johannsson, M. Kaess, B. Englot, F. Hover, and J. Leonard, "Imaging sonar-aided navigation for autonomous underwater harbor surveillance," in 2010 IEEE/RSJ International Conference on Intelligent Robots and Systems, 2010.

[3] L. Wallace, A. Lucieer, C. Watson, and D. Turner, "Development of a UAV-LiDAR System with Application to Forest Inventory," Remote Sensing, vol. 4, no. 12, pp. 1519–1543, 2012.

[4] D. R. Yoerger, M. Jakuba, A. M. Bradley, and B. Bingham, "Techniques for Deep Sea Near Bottom Survey Using an Autonomous Underwater Vehicle," Int. J. Rob. Res., vol. 26, no. 1, pp. 41–54, 2007.

[5] M. F. Fallon, M. Kaess, H. Johannsson, and J. J. Leonard, "Efficient AUV navigation fusing acoustic ranging and side-scan sonar," in 2011 IEEE International Conference on Robotics and Automation, 2011.

[6] M. V. Jakuba et al., "Long-baseline acoustic navigation for under-ice autonomous underwater vehicle operations," Journal of Field Robotics, vol. 25, no. 11–12, pp. 861–879, 2008.

[7] G. Antonelli, F. Arrichiello, S. Chiaverini, and G. S. Sukhatme, "Observability analysis of relative localization for AUVs based on ranging and depth measurements," in 2010 IEEE International Conference on Robotics and Automation, 2010.

[8] D. Viegas, P. Batista, P. Oliveira, and C. Silvestre, "Position and velocity filters for intervention AUVs based on single range and depth measurements," in 2012 IEEE International Conference on Robotics and Automation, 2012.

[9] C.-Y. Kim, D. Song, Y. Xu, and J. Yi, "Localization of multiple unknown transient radio sources using multiple paired mobile robots with limited sensing ranges," in 2011 IEEE International Conference on Robotics and Automation, 2011.

[10] G. Griffiths, Technology and Applications of Autonomous Underwater Vehicles. CRC Press, 2002.

[11] S. Arnon, "Underwater optical wireless communication network," Opt. Eng., vol. 49, no. 1, p. 015001, 2010.

[12] L. L. Beranek, and T. Mellow, [Acoustics: sound fields and transducers] Academic Press, Waltham, MA, 2012.

[13] S. E. Webster, R. M. Eustice, H. Singh, and L. L. Whitcomb, "Preliminary deep water results in single-beacon one-way-travel-time acoustic navigation for underwater vehicles," in 2009 IEEE/RSJ International Conference on Intelligent Robots and Systems, 2009.

[14] H. Bülow and A. Birk, "Spectral registration of noisy sonar data for underwater 3D mapping," Auton. Robots, vol. 30, no. 3, pp. 307–331, 2011.

[15] P. Jonsson, I. Sillitoe, B. Dushaw, J. Nystuen, and J. Heltne, "Observing using sound and light – a short review of underwater acoustic and video-based methods," Ocean Sci. Discuss., vol. 6, no. 1, pp. 819–870, 2009.

[16] C. D. Mobley, Light and Water: Radiative Transfer in Natural Waters. 1994.

[17] J. Michel, T. Oppikofer, A. Abellan, M. Derron, A. Loye, R. Metzger and A. Pedrazzini, "Use of LIDAR in landslide investigations: a review," Natural Hazards., vol. 61, no.1, pp.5-28, 2012.

[18] J. Sun, E. Timurdogan, A. Yaacobi, E. S. Hosseini, and M. R. Watts, "Large-scale nanophotonic phased array," Nature, vol. 493, no. 7431, pp. 195–199, Jan. 2013.

[19] A. Yaacobi, J. Sun, M. Moresco, G. Leake, D. Coolbaugh, and M. R. Watts, "Integrated phased array for wide-angle beam steering," Optics Letters, vol. 39, no.15, pp. 4575-4578, 2014.

[20] X. Lee and C. Wang, "Optical design for uniform scanning in MEMS-based 3D imaging lidar," Appl. Opt., vol. 54, no. 9, pp. 2219–2223, Mar. 2015.

[21] A. Kasturi, V. Milanovic, B. H. Atwood, and J. Yang, "UAV-borne lidar with MEMS mirror-based scanning capability," Laser Radar Technology and Applications XXI., vol.9832, pp.98320M, 2016.

[22] C.-H. Huang, J. Yao, L. V. Wang, and J. Zou, "A water-immersible 2-axis scanning mirror microsystem for ultrasound andha photoacoustic microscopic imaging applications," Microsyst. Technol., vol. 19, no. 4, pp. 577–582, 2012.

[23] S. Xu, C.-H. Huang, and J. Zou, "Microfabricated water-immersible scanning mirror with a small form factor for handheld ultrasound and photoacoustic microscopy," J. Micro/Nanolithogr. MEMS MOEMS, vol. 14, no. 3, p. 035004, 2015.

[24] S. Xu, C.-H. Huang, and J. Zou, "A two-axis water-immersible MEMS scanning mirror for scanning optical and acoustic microscopy," in SPIE MOEMS and Miniaturized Systems XV, 2016.

[25] J.-Y. Kim, C. Lee, K. Park, G. Lim, and C. Kim, "Fast optical-resolution photoacoustic microscopy using a 2-axis water-proofing MEMS scanner," Sci. Rep. vol. 5, pp. 7932, 2015.